RNA (2001), *7*:692–701. Cambridge University Press. Printed in the USA.

Ribosomal protein L5 has a highly twisted concave surface and flexible arms responsible for rRNA binding

TAKASHI NAKASHIMA,[1] MIN YAO,[1,2] SHUNSUKE KAWAMURA,[3] KENTA IWASAKI,[3] MAKOTO KIMURA,[3] and ISAO TANAKA[1,2]

[1]Division of Biological Sciences, Graduate School of Science, Hokkaido University, Sapporo 060-0810, Japan
[2]Division of Bio-Crystallography Technology, RIKEN Harima Institute/Spring-8, Kouto, Mikazuki, Sayo, Hyogo 679-5148, Japan
[3]Laboratory of Biochemistry, Faculty of Agriculture, Kyushu University, Fukuoka 812-8581, Japan

ABSTRACT

Ribosomal protein L5 is a 5S rRNA binding protein in the large subunit and plays an essential role in the promotion of a particular conformation of 5S rRNA. The crystal structure of the ribosomal protein L5 from *Bacillus stearothermophilus* has been determined at 1.8 Å resolution. The molecule consists of a five-stranded antiparallel β-sheet and four α-helices, which fold in a way that is topologically similar to the ribonucleoprotein (RNP) domain. The molecular shape and electrostatic representation suggest that the concave surface and loop regions are involved in 5S rRNA binding. To identify amino acid residues responsible for 5S rRNA binding, we made use of Ala-scanning mutagenesis of evolutionarily conserved amino acids occurring in the β-strands and loop regions. The mutations of Asn37 at the β1-strand and Gln63 at the loop between helix 2 and β3-strand as well as that of Phe77 at the tip of the loop structure between the β2- and β3-strands caused a significant reduction in 5S rRNA binding. In addition, the mutations of Thr90 on the β3-strand and Ile141 and Asp144 at the loop between β4- and β5-strands moderately reduced the 5S rRNA-binding affinity. Comparison of these results with the more recently analyzed structure of the 50S subunit from *Haloarcula marismortui* suggests that there are significant differences in the structure at N- and C-terminal regions and probably in the 5S rRNA binding.

Keywords: 5S rRNA; RNA-binding protein; X-ray structure

INTRODUCTION

There is growing evidence that RNA molecules play essential roles in biological processes of living cells, such as pre-mRNA splicing in the spliceosome (Burge et al., 1999) and peptide-bond formation in the ribosome (Nissen et al., 2000). RNA molecules usually perform these functions in close association with RNA-binding proteins, and thus the RNA–protein interaction is central to understanding a wide range of biological processes.

5S rRNA, which has approximately 120 nt, is a ubiquitous component in the large ribosomal subunit and occurs as a ribonucleoprotein particle within the central protuberance of the subunits (Bogdanov et al., 1995; Dallas et al., 1995). The physiological role of the 5S rRNA protein particle in the ribosome is still not well understood. In thermophilic bacterium *Thermus aquaticus*, 5S rRNA protein particle has been reported to play a key role in assembling an active peptidyltransferase center by correctly positioning functionally important segments of domains II and IV of 23S rRNA (Khaitovich & Mankin, 1999). It has been further reported that 5S rRNA may participate in signal transmission between the two functional centers (the peptidyltransferase center and the translocation center) in the *Escherichia coli* ribosomes (Sergiev et al., 2000). In contrast to these findings, 50S subunits reconstituted in the absence of 5S rRNA retained significant peptidyltransferase activity in the *E. coli* (Schulze & Nierhaus, 1982) and *Bacillus stearothermophilus* (Green & Noller, 1999) ribosomes.

In spite of the uncertainty about the physiological role, the 5S rRNA protein particle has long been a good model system for studying the protein–RNA interaction, because it is easily isolated and reconstituted (Horne &

Reprint requests to: Isao Tanaka, Division of Biological Sciences, Graduate School of Science, Hokkaido University, Sapporo 060-0810, Japan; e-mail: tanaka@castor.sci.hokudai.ac.jp.

Erdmann, 1972). The number of proteins associated with 5S rRNA varies from one to three depending on the source of the ribosome. In *E. coli*, 5S rRNA is complexed with three proteins, L5, L18, and L25 (Chen-Schmeisser & Garret, 1977). Extensive studies using the footprinting method against ribonucleases and chemical reagents have identified a number of possible binding sites for individual proteins on the *E. coli* 5S rRNA (Zimmermann & Erdmann, 1978; Douthwaite et al., 1979; Garrett & Noller, 1979; Huber & Wool 1984; Shpanchenko et al., 1996). The crystal structures of a 62-nt domain of 5S rRNA and a duplex dodecamer encompassing an internal loop E have been determined at 3.0 Å and 1.5 Å resolutions, respectively (Correll et al., 1997). Furthermore, the three-dimensional structures of L25 from *E. coli* have been analyzed with and without the RNA fragment corresponding to loop E of 5S rRNA (Stoldt et al., 1998, 1999; Lu & Steitz, 2000).

In addition to *E. coli*, the 5S rRNA protein particle from *B. stearothermophilus* has been isolated and characterized (Horne & Erdmann, 1972). Two proteins (*Bst*L5 and *Bst*L18) from the *B. stearothermophilus* ribosome that can bind to 5S rRNA were identified and correlated with L5 and L18 from *E. coli*. The proteins *Bst*L5 and *Bst*L18 consist of 179 and 120 amino acid residues and share 59 and 53% identical residues with *E. coli* homologs, respectively (Kimura & Kimura, 1987). A ribonuclease T1 hydrolysis experiment showed that *Bst*L5 and *Bst*L18 protect the nucleotide sequences 18–57 and 58–100 of *E. coli* 5S rRNA, respectively (Zimmermann & Erdmann, 1978). To gain more insight into the interaction of 5S rRNA and proteins, and also to facilitate structural analysis of the intact 50S subunits, we attempted to crystallize the recombinant proteins *Bst*L5 and *Bst*L18 overexpressed in *E. coli* cells. Although no suitable crystals for *Bst*L18 have been available thus far, the *Bst*L5 crystals were grown under an appropriate condition.

In the present study, we determined the crystal structure of *Bst*L5 at 1.8 Å resolution by means of the multiwavelength anomalous diffraction method using a selenomethionyl derivative. The molecule has a ribonucleoprotein (RNP) motif for RNA recognition. On the basis of the crystal structure, we attempted to identify amino acid residues responsible for 5S rRNA binding by site-directed mutagenesis. These results were compared with the more recently analyzed structure of the 50S subunit of the *Haloarcula marismortui* ribosome (Ban et al., 2000).

RESULTS AND DISCUSSION

Structure description

The ribosomal protein L5 from *B. stearothermophilus* (*Bst*L5) consists of 179 amino acid residues. The crystal structure of *Bst*L5 was solved by the multiple wavelength anomalous diffraction (MAD) method and refined against 1.8 Å resolution native data using the CNS program (see Materials and Methods). Two molecules in the asymmetric unit (referred to as A and B) have slightly different conformations at the loop regions. The current model includes all 179 residues for both A and B molecules, plus 376 water molecules. A stereo view of the overall structure of *Bst*L5 is shown in Figure 1. The structure is of the α/β type, consisting of a five-stranded antiparallel β-sheet and four α-helices. The connectivity scheme of the molecule is α1-β1-α2-β2-β3-α3-β4-β5-α4, and the secondary structure of *Bst*L5, as defined by the DSSP program (Kabsch & Sander, 1983) is given in Figure 2. The folding topology of the central part of *Bst*L5 (β1-α2-β2-β3-α3-β4), which excludes α1 (resides 4–19), β5 (residues 163–174), and α4 (residues 163–174) at the N- and C-termini, has some similarities to the ribonucleoprotein (RNP) family of proteins (see, e.g., Burd & Dreyfuss, 1994). Unlike typical RNP (which is also referred to as RNA recognition motif (RRM)), a β-stand (β5) is inserted between β4 and β1, forming an antiparallel five-stranded β-sheet rather than a four-stranded sheet. The concave shape of the β-sheet is reinforced by the hydrophobic interactions on the back side of the β-sheet where α-helical segments (α2 and α3) and the proximal part of the loop (β4–β5) pack against the β-sheet, forming a well-extended hydrophobic cluster. The surface representation of the electrostatic potential clearly shows that the concave surface of the molecule is positively charged, whereas the backside is neutral (Fig. 3).

N- and C-terminal α-helices (α1 and α4) together with helix 3 (α3) form a hydrophobic cluster at one edge of the β-sheet. Because of this interaction, both termini of the peptide chain are well defined in the electron density. As the sequence comparison (Fig. 2) shows that the amino acid sequences at N- and C-terminal regions are not conserved between eubacteria and others, it appears this structure is specific for eubacteria. At the opposite edge of the β-sheet are the loop regions. Loop (β2–β3) peels off from the β-sheet surface, giving the impression that the molecule has a concave shape. The electron density corresponding to this loop region is the least well defined in both A and B molecules. The electron density corresponding to loop (β1–α2) is also weak in molecule B, but it is well defined in molecule A, probably due to the contacts with neighboring molecules. These poorly defined loops of *Bst*L5 are presumably flexible and may interact with rRNA in the ribosome, thereby fixing the conformations. The structure of loop (β4–β5) is well ordered because of the hydrophobic interactions along the proximal part of the loop (especially at residues Ile137 and Phe138 with Phe99 of α3). The role of this loop may not be one related to rRNA binding, but rather structural in nature.

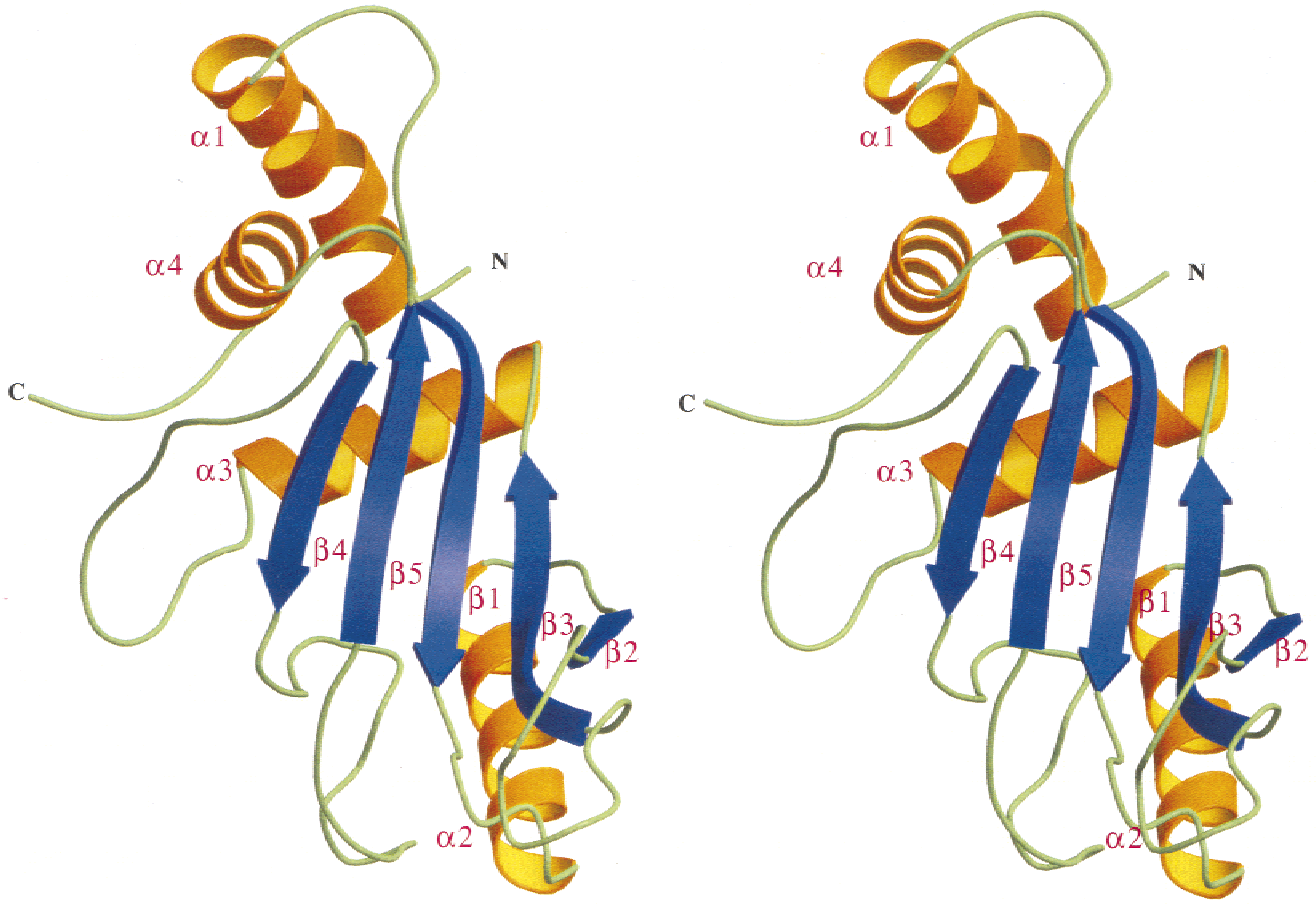

FIGURE 1. A stereoscopic drawing of the ribosomal protein L5 from *B. stearothermophilus*.

Similar structures

The folding topology of *Bst*L5 indicates that this molecule can be classified into the ribonucleoprotein (RNP) family of RNA-binding proteins, members of which control many aspects of RNA processing in eukaryotic cells (Burd & Dreyfuss, 1994). The RNP family of proteins includes, among others, the U1 small nuclear ribonucleoprotein particle (U1 snRNP). The three-dimensional structure of the N-terminal RNA-binding domain of U1 snRNP A (U1A), a member of the RNP, was determined in 1990 (Nagai et al., 1990). The structure is characteristics of the split $\beta\alpha\beta\beta\alpha\beta$ secondary structural elements that form a four-stranded antiparallel β-sheet packed against the two perpendicularly oriented α-helices. Identical folding topology has been found in the ribosomal protein S6, and variants have been found in L1, L6, L7/L12, L9, L22, and L30 (see, e.g., Ramakrishnan & White, 1998). Actually this is the most frequently occurring folding motif in the ribosomal proteins. However, none has entirely the same folding topology, and no sequence similarity has been detected within these molecules. Despite the topological resemblance between *Bst*L5 and the RNP family of proteins, the structure of *Bst*L5 is distinct from these molecules in its overall dimensions (*Bst*L5 is much larger). Although it is tempting to speculate that the ribosomal protein is at least remotely evolutionarily related to the RNP family of proteins, the complete lack of sequence similarity, including the canonical sequence of RNP, suggests that the relationship between these molecules is extremely distant if present at all.

Possible RNA-binding site

It is now believed that the primary role of ribosomal proteins is to direct the folding and to stabilize the tertiary structure of the ribosomal RNA. The three-dimensional structures of the ribosomal proteins determined thus far have shown that the ribosomal proteins have a well-extended hydrophobic core structure and protruding flexible arm regions. The sequence comparisons of the ribosomal proteins from many different species have revealed that the flexible loop or arm regions quite often contain mostly conserved amino residues. Because these flexible parts have almost no interactions within the molecule, the conservation of amino acids in these regions is indicative that they have con-

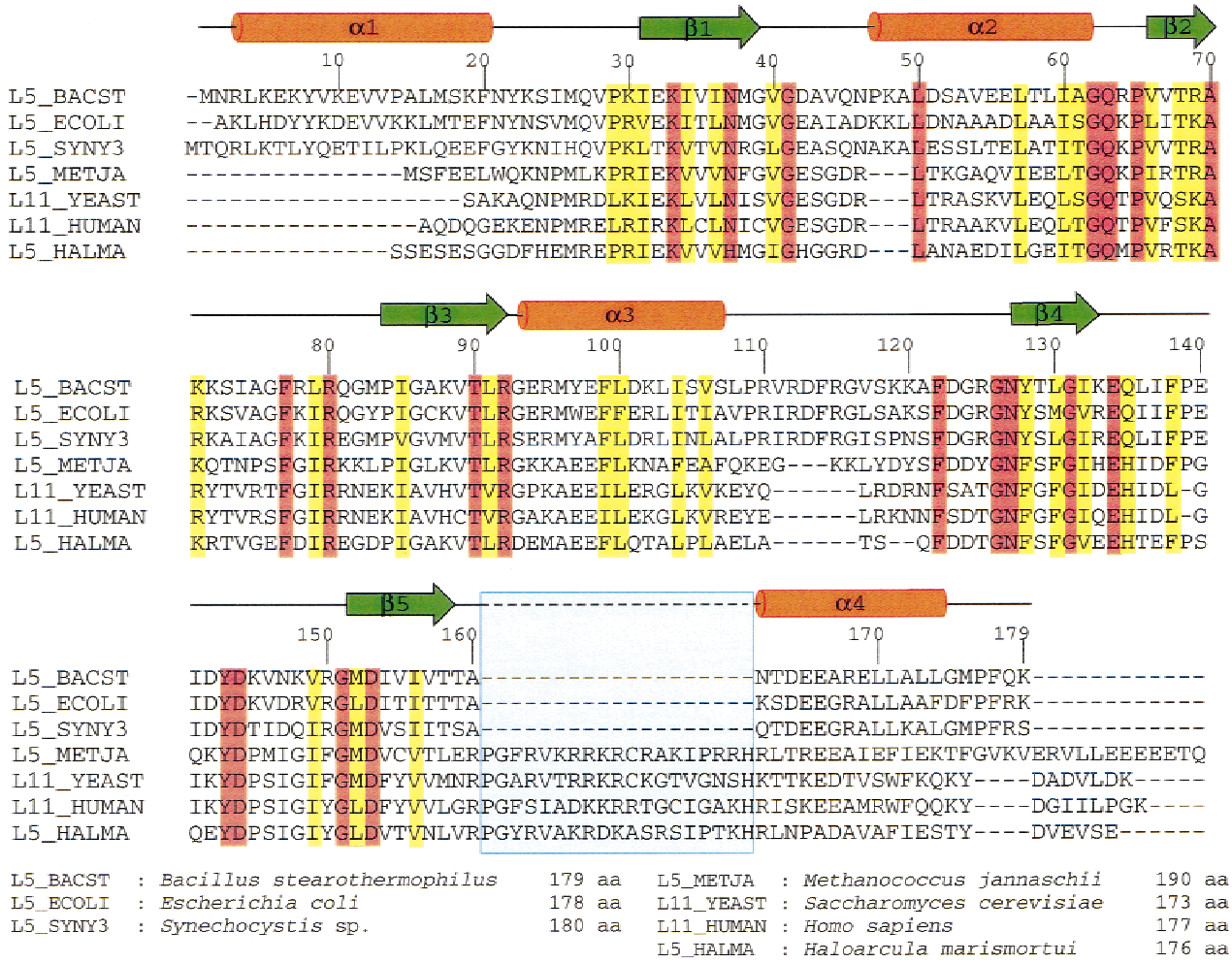

FIGURE 2. Sequence comparison of the ribosomal protein L5. The amino acid residues are shaded as follows: completely identical (red), conserved change (yellow). The secondary structure elements indicated are those defined by the present work for *Bst*L5 using the DSSP program (Kabsch & Sander, 1983). The alignment at the C-terminal portion including α4 is based on the tertiary structures of *Bst*L5 (present study) and *Hma*L5 (Ban et al., 2000). Loop region that is unique in archaea and eukaryote is boxed (blue).

tact with other (possibly RNA) molecules, thereby playing an important role. The electrostatic surface potential representation also allows us to estimate functional regions for this class of molecules. Quite often, the ribosomal proteins have surface patches where positively charged residues are localized. These regions are believed to create a contact surface with rRNA.

The ribosomal protein L5 is the primary 5S rRNA binding protein. The 5S rRNA is a small RNA component (120 nt long) of the 50S subunit of the ribosomes. Its secondary structure is well characterized, having five helices (I to V) and five loops (A to E). The primary target site of the L5 protein is at loops B and C. From the structure of *Bst*L5, we attempted to predict the RNA-binding site. The electrostatic potential surface representation showed that the concave surface together with the arm region contains the mostly positively charged residues, suggesting that these are the primary RNA-binding sites. The structural similarity between *Bst*L5 and the RNP family of proteins supported this hypothesis. The three-dimensional structure analysis of U1A complexed with the 21-nt RNA hairpin has shown that U1A binds with the 10-nt loop of the RNA hairpin that forks from the stem region and adopts an open structure (Oubridge et al., 1994).

A comparison of amino acid sequences of the L5 family of proteins has indeed revealed a number of evolutionarily conserved residues in β-strands and loop regions. To consider the role of these amino acids in RNA binding, we made use of Ala-scanning site-directed mutagenesis. The residues replaced were Asn37, Thr90, and Asp153 in the β-strands and Gln63, Phe77, Arg80, Ile141, Tyr143, and Asp144 in the loop regions.

All mutants were expressed in *E. coli* BL21 (DE3) cells using the expression vector pET-22b and were purified by ion-exchange chromatography on SP-Sepharose, as described for the wild type. Throughout the purification process, all mutants behaved like the

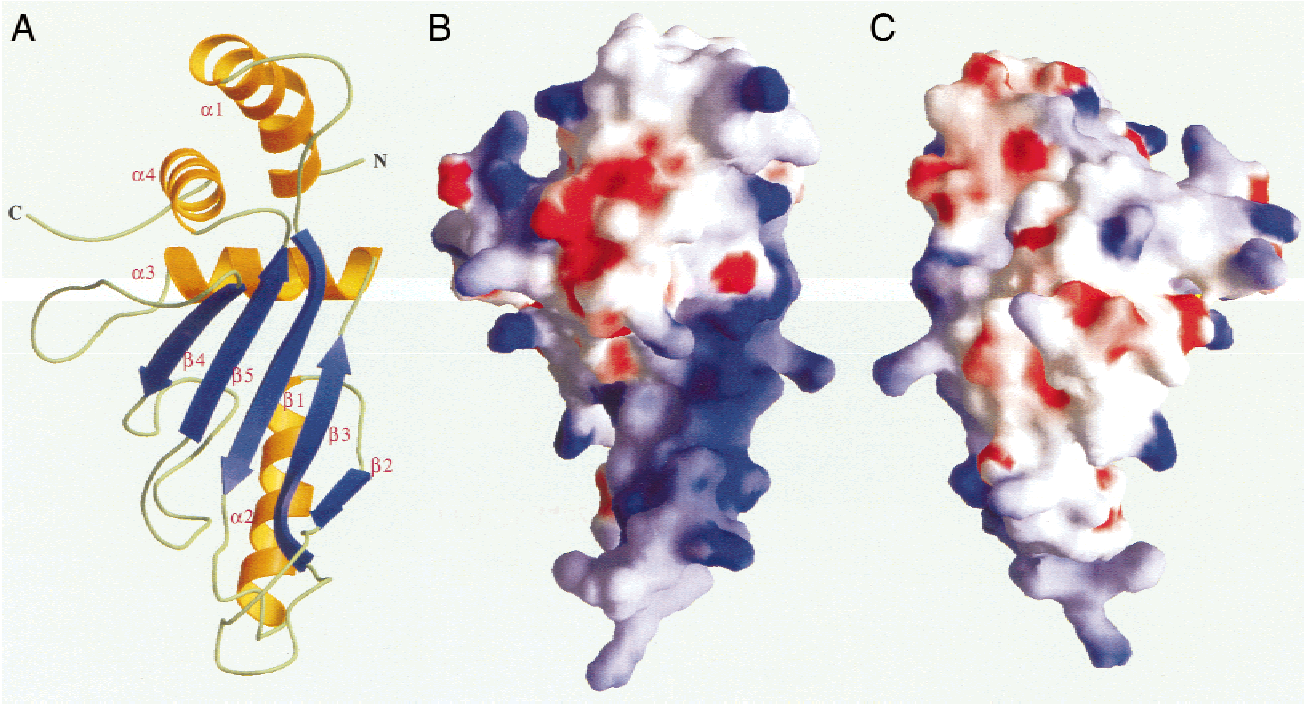

FIGURE 3. Surface representation of the electrostatic potential of *Bst*L5 as calculated by GRASP (Nicholls et al., 1991). The surface potential is displayed as a color gradient from red (negative) to blue (positive). **A,B:** Molecular surface of the rRNA-binding region showing the relatively strong electropositive character. **C:** The view after 180 deg rotation from **A** and **B**.

wild type and exhibited almost the same elution pattern as L5. The structural integrity of the mutant proteins was evaluated by comparing their CD spectra in the far-ultraviolet region (200–250 nm) with that of the wild-type L5. This analysis showed that the CD spectra of all mutants were approximately identical to that of the wild type, indicating that replacements of amino acids by Ala do not seem to affect the integrity of the protein structure. These mutant proteins were characterized with respect to their binding potency, based on the results of a filter-binding assay. The apparent binding constants of the mutant proteins obtained in this analysis are given in Table 1. Mutations of Asn37, Gln63, and Phe77 (N37A, Q63A, and F77A) resulted in 25-, 12.5-, and 8.3-fold decreases, respectively, in binding constants (K), compared with the wild type (Table 1). In contrast, the Y143A and D153A mutations had no significant effect on the RNA-binding affinity.

TABLE 1. Binding constants of *Bst*L5 and its mutants.

Mutant	K (μM^{-1})	Relative K
Wild type	5.0	1.0
N37A	0.2	0.04
Q63A	0.4	0.08
F77A	0.6	0.12
R80A	3.6	0.72
T90A	1.2	0.24
I141A	2.8	0.56
Y143A	4.6	0.92
D144A	3.3	0.66
D153A	4.9	0.98

Figure 4 shows the main-chain folding with side chains of the amino acid residues analyzed in the present study. The N37A and T90A mutations at the β1 and β3 strands, respectively, had a significant effect on the 5S rRNA-binding activity. Additionally, the mutations Q63A and F77A that lay on top of the α2–β2 and β2–β3 loops, respectively, also reduced the 5S RNA-binding activity. These results indicate that Asn37 and Thr90 at the antiparallel β-strands (β1 and β3) and Gln63 and Phe77 at the loops (α2–β2 and β2–β3) are essential for RNA binding. This result indicates that although there is little sequence similarity between *Bst*L5 and the RNP domain, the essential amino acid residues for RNA binding occupy similar surfaces in the proteins. As described in the structure description, the β2–β3 loop has the weakest electron density. It is further known that the Phe77 residue is extremely susceptible to chymotrypsin, suggesting that it is very flexible (M. Kimura, unpubl. results). It is thus likely that this region of the molecule can become ordered on RNA binding.

It was further found that the Ile141 and Asp144 mutations at the β4–β5 loop cause a moderate reduction in RNA binding. In the X-ray structure analysis, the

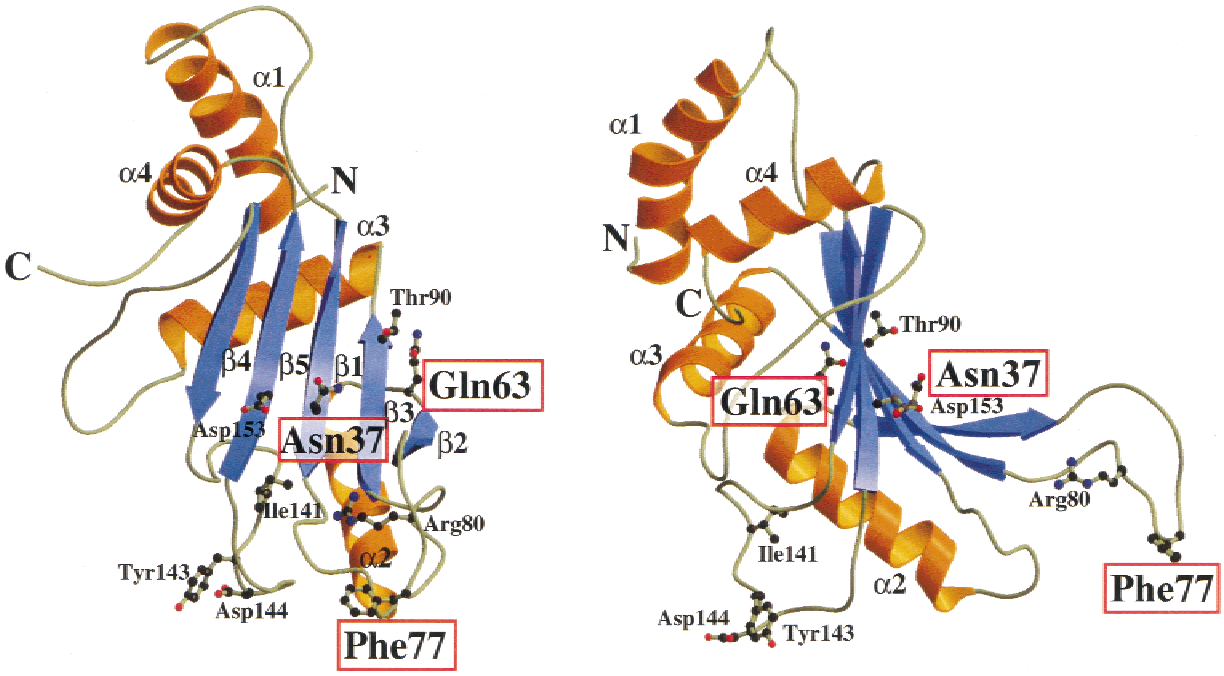

FIGURE 4. Orthogonal view of *Bst*L5 showing residues subjected to mutation experiment. The residues that were shown to be important for 5S rRNA binding are emphasized by a red box.

β4–β5 loop had a strong electron density, suggesting its rigid conformation. It is thus unlikely that the β4–β5 loop is directly involved in 5S rRNA binding, but rather that it participates in stabilizing the β-sheet structure. The observed reduction in 5S rRNA binding activity is probably due to a slight structural perturbation on the back side of the antiparallel β-sheet.

Comparison with the L5 structure in the 50S subunit of *H. marismortui*

During preparation of this article, the structure of the 50S subunit from *H. marismortui* was published (Ban et al., 2000), which enables us to compare our L5 structure (and mutagenesis data) with that of the 50S subunit of this halo bacteria. Figure 5 provides a comparison of the molecular structures of *Bst*L5 and L5 of the 50S subunit from *H. marismortui* (*Hma*L5). Although two loop regions (between β1 and α2 and between β4 and β5) of *Hma*L5 are not defined in the crystal, it is still evident that the two molecules have the same folding topology. The obvious differences are at the N- and C-terminal regions. As mentioned above, these regions are the least conserved in the amino sequences (Fig. 2), and the alignment at the C-terminal region, including α4, is not possible without reference to these tertiary structures. As shown in Figure 2, *Hma*L5 and *Bst*L5 share approximately 30% identical residues, and *Bst*L5 has an N-terminal extension with 13 amino acids, whereas *Hma*L5 has a long insertion with 20 amino acids between β5 and α4 in *Bst*L5. The structures of the two molecules are similar, even with this sequence difference in the residues, possessing the same elements of a secondary structure. The differences in the α-carbon tracings occur primarily due to the differences in length of the two proteins. The N-terminal α-helix of *Bst*L5, which is completely missing in *Hma*L5, should be located at the particle surface and exposed to the solvent. The C-terminal insertion found in *Hma*L5 forms a long extra loop and fills the space between 5S rRNA and 23S rRNA (Fig. 5). As the sequence alignment suggests (Fig. 2), this interaction seems to be unique in archaebacteria as well as in eukaryotic ribosome.

The crystal structure of *Hma*L5 shows that protein L5 strongly binds not only 5S rRNA but also 23S rNA (at helix 86). When examining 5S rRNA binding sites on *Hma*L5, 5S rRNA predominantly interacts with the antiparallel β-sheet, which is consistent with the result concerning the mutation, that defined the antiparallel β-sheet, composed of the β1, β2, and β3 strands, as one of the 5S rRNA binding sites. The present mutational study suggests that Phe77 located at the loop between the β2 and β3 strands is involved in 5S rRNA binding. However, the structure of *Hma*L5 of the 50S subunit shows that the loop containing the conserved Phe is located far from 5S rRNA and has no interaction with it. At present, we have no clear explanation as to

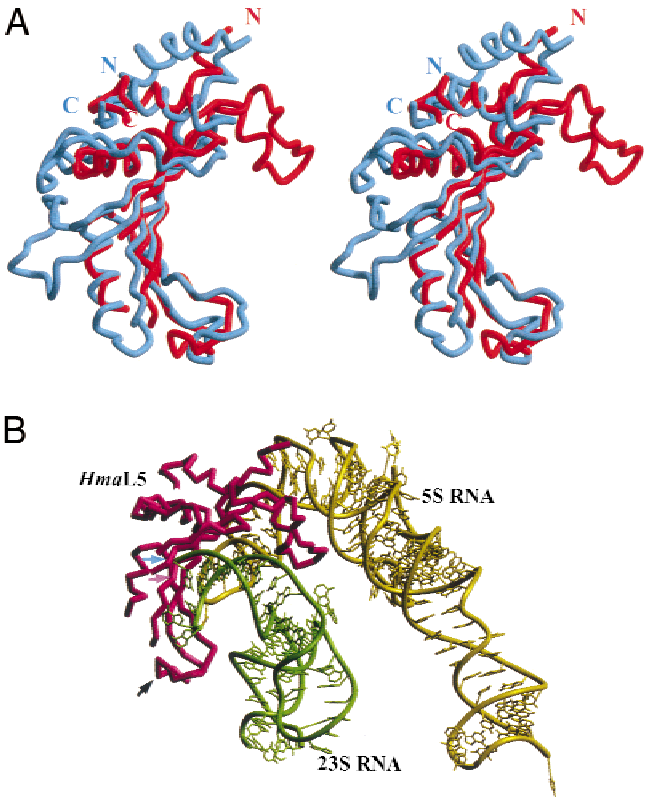

FIGURE 5. A: Stereo view of the superposition of the molecular structures of L5 from *B. stearothermophilus* (*Bst*L5: blue) and that in the 50S subunit of *H. marismortui* (*Hma*L5: red; Ban et al., 2000). The α-carbon tracing of *Hma*L5 is incomplete for the two loop regions at the back of the concave surface. The two molecules are different at the N- and C-terminal regions. At the N-terminus, *Bst*L5 has 13 extra residues that form the α-helix, and at the C-terminal region the inserted 20 residues of *Hma*L5 form extra loop characteristic of the archaea and eukaryote. **B:** This loop penetrates into the gap between 5S rRNA and 23S rRNA and fills the space (Ban et al., 2000). Mutation positions that affect 5S rRNA binding in *B. stearothermophilus* are marked by arrows (blue: Gln63, purple: Asn37, and black: Phe77).

why the mutation of Phe77 in *Bst*L5 affects 5S rRNA binding activity. One possibility is that although Phe77 is not directly involved in the interaction between 5S rRNA in the final structure, it may be involved in the interaction during the process of forming the 5S rRNA structure. Another possibility is that the interaction of the L5 protein and 5S rRNA in eubacterial ribosome may be different from that within the archaebacterial (*H. marismortui*) ribosome. It has been reported that the structure of 5S rRNA in complex with L5, L18, and L25 differs from that in the 50S ribosome subunit (Shpanchenko et al., 1998). These assumptions will be addressed in a structure analysis of 5S rRNA complexed with *Bst*L5 and *Bst*L18 that is now in progress in our laboratories.

MATERIALS AND METHODS

Preparation of the recombinant BstL5

For the overexpression of *Bst*L5, its entire gene was amplified by polymerase chain reaction from a genomic DNA from *B. stearothermophilus* and placed under the control of the T7 phage promoter on the expression plasmid pET-22b. Expression of the *Bst*L5 gene in *E. coli* BL21 (DE3) and subsequent purification of the resulting protein was performed as follows. The *E. coli* cells were harvested by centrifugation, washed, and disrupted using a French press in buffer RP (50 mM Tris-HCl, pH 7.5, 1 mM EDTA, 1 mM DTT, 0.1 mM PMSF). Cell debris was removed by centrifugation for 20 min at 20,000 $\times$ *g*. The supernatant was loaded on a SP-Sepharose FF column equilibrated with the buffer RP. After washing, the protein was eluted with a linear gradient from 0.2 to 0.8 M NaCl in the buffer RP. The fractions were analyzed by SDS-PAGE. The purity of the protein was confirmed by direct N-terminal amino acid sequencing and MALDI-TOF MS analyses. The N-terminal sequencing provided a single sequence, Met-Asn-Arg-Leu-Lys, indicating that the recombinant *Bst*L5 had an amino acid sequence identical to that of the authentic *Bst*L5. The molecular weight, determined by MALDI-TOF MS analysis, was 20,089 Da, which coincided well with the calculated value (20,163 Da) of the *Bst*L5. To test whether the *Bst*L5 was correctly folded into an active conformation, the capability of the protein to bind 5S rRNA was examined by a filter-binding assay, as described previously (Harada et al., 1998). For this purpose, a total length of *B. stearothermophilus* 5S rRNA was produced in the presence of ^{35}S-UTP using T7-based in vitro runoff transcription with a plasmid template (pGEM-T vector). The resulting product was treated with DNase I and purified by ethanol precipitation. Under the condition used, the *Bst*L5 bound 5S rRNA with an apparent binding constant of 5.0 μM^{-1}, which is comparable to those of other ribosomal RNA binding proteins (Schwarzbauer & Craven, 1981).

Crystallization and X-ray data collection

The purified protein was dialyzed against distilled water and concentrated to 10 mg/mL by means of a Centricon concentrator (Amicon). Crystallization was carried out at 18 °C by the hanging-drop vapor diffusion technique. The crystal screens I and II (Hampton Research, California) were used to search for the crystallization conditions of *Bst*L5. The crystals were obtained under several conditions, including numbers 4, 7, and 41 of crystal screen I, and number 38 of crystal screen II. Crystallization was optimized under these conditions. The best crystal of *Bst*L5 was obtained at 18 °C from 0.1 M HEPES, pH 8.0, containing 16% polyethylene glycol 8000 and 10% 2-methyl-2-,4-pentanediol. Crystals were grown within a few days to a size of up to 0.2 $\times$ 0.4 $\times$ 0.6 mm^3 at 18 °C. Subsequently, a selenomethionine (Se-Met) derivative for *Bst*L5 was prepared, and its crystals were produced under conditions identical to those described for the native *Bst*L5.

X-ray diffraction data sets for native *Bst*L5 and Se-Met *Bst*L5 were collected at 100 K on a MAR CCD detector at the BL44B2 and BL41XU stations of SPring-8. The crystals were soaked stepwise from 10 to 20% MPD in the reservoir solution for a few minutes, suspended on a loop in a thin liquid

TABLE 2. The summary of data collection.

		MAD data		
	Native	Peak	Edge	Remote
Wavelength (Å)	0.70000	0.979155	0.979467	0.90000
Resolution (Å)	40–1.8 (1.9–1.8)	40–2.1 (2.2–2.1)	40–2.1 (2.2–2.1)	40–2.0 (2.1–2.0)
No. of obs. reflections	252,800	172,941	169,984	193,341
Unique reflections	37,507	24,745	24,652	28,428
Completeness (%)	97.7 (96.6)	99.6 (99.6)	99.4 (99.4)	99.3 (99.3)
Averaged redundancy	6.7 (3.4)	7.0 (7.2)	6.9 (7.1)	6.8 (7.0)
Averaged I/σ (I)	7.6 (3.7)	6.0 (2.5)	5.8 (2.6)	5.5 (2.7)
R_{meas} (%)[a]	5.0 (23.9)	7.0 (29.1)	6.4 (24.5)	6.3 (25.2)

Values in parentheses are for the outermost resolution shell.

[a] $R_{meas} = \sum_h [m/(m-1)]^{1/2} \sum_j |\langle I \rangle_h - I_{hj}| / \sum_h \sum_j I_{hj}$, where $\langle I \rangle_h$ is the mean intensity of symmetry-equivalent reflections and m is redundancy.

film of stabilizing solution, and directly frozen at 100 K in a cold nitrogen gas stream with a Cryostream Cooler. The crystals of both native and Se-Met *Bst*L5 belong to the space group C2, but with slightly different cell dimensions. The cell dimensions of the native *Bst*L5 were a = 138.65 Å, b = 49.22 Å, c = 68.93 Å, and β = 117.30°, and those of Se-Met *Bst*L5 were a = 139.51 Å, b = 49.54 Å, c = 69.23 Å, and β = 117.32°. By assuming two *Bst*L5 molecules in the asymmetric unit, V_M was calculated to be 2.65 Å^3/Da, which is within the range observed for protein crystals (Matthews, 1968). The solvent content of the crystals was calculated to be 53.7%. The results of the data reduction are summarized in Table 2. The reflections were indexed and integrated using MOSFLM (Leslie, 1993) and scaled and reduced using SCALA (Evans, 1997).

Structure determination and refinement

Fourteen of the 16 total selenium sites were located by the program package SOLVE (Terwilliger & Berendzen, 1999). Heavy-atom parameter refinement and phase calculations were carried out using the program SHARP (La Fortelle & Bricogne, 1997). The operators of noncrystallographic symmetry (NCS) were obtained by LSQKAB (Kabsch, 1976) and improved by IMP of the Uppsala program package (Kleywegt & Read, 1997) using eight sites of 14 selenium atoms. Because electron-density features corresponding to the two independent molecules were somewhat different, the initial electron density map was not subjected to NCS averaging but was rather improved only by solvent flattening with SOLOMON (Abrahams & Leslie, 1996) using the procedure in the SHARP program. The phasing statistics are summarized in Table 3. The atomic model was built using the graphics program O (Jones et al., 1991). The model of Se-Met *Bst*L5 was refined against the remote data for the Se-Met *Bst*L5 crystal with the CNS program (Brünger et al., 1998) using positional and temperature factor refinement followed by a few cycles of simulated annealing refinement.

Because the selenomethionyl derivative was not isomorphous with the native crystal, a native *Bst*L5 model was obtained by molecular replacement using program AMORE (Navaza, 1994). The phases were improved by NCS averaging using the programs DM (Cowtain & Main, 1996) and SIGMAA (Read, 1986). The model was rebuilt on the electron density map by the O program. At the current stage of refinement, the model has an R-factor of 21.5%, and free R-factor of 25.9% for the data between 10 Å and 1.8 Å, including 179*2 residues for crystallographically independent molecules, and 376 water molecules. The refinement statistics are summarized in Table 4. The coordinates will be deposited in the Protein Data Bank (Abola et al., 1997).

TABLE 3. Phasing statistics.

	Remote		Peak		Edge	
Data	Dispersive	Bijvoet	Dispersive	Bijvoet	Dispersive	Bijvoet
R_{Cullis}[a]			0.5267		0.5923	
Phasing power[b]		2.188	3.330	2.540	3.327	1.541
FOM[c]	0.6681					
FOM after SOLOMON	0.8379					

[a] R_{Cullis} is the mean residual lack of closure error divided by dispersive difference. Values are for centric reflections.

[b] Phasing power of the dispersive is the root mean square of F_H/E where F_H is the dispersive difference of F_H and E is the lack of closure error. Phasing power of the Bijvoet is as for phasing power of the dispersive except that F_H is the Bijvoet difference of F_H.

[c] FOM is the mean figure of merit.

TABLE 4. Refinement statistics.

Resolution range (Å)	10–1.8
Number of reflections	37,123 ($F > 2\sigma$)
Residues included	179*2
Number of non-hydrogen atoms	2,826
Number of water molecules	376
R-factor (%)[a]	21.5
R_{free}-factor (%)[b]	25.9
Average B factor (Å^2)	41.96
Rms deviations	
bond lengths (Å)	0.0115
bond angles (°)	1.48
dihedral angles (°)	22.6

[a] R-factor $= \sum|F_{obs} - F_{cal}|/\sum F_{obs}$, where F_{obs} and F_{cal} are observed and calculated structure factor amplitudes.

[b] R_{free}-factor value was calculated as for R-factor but using only an unrefined subset of reflections data (10%).

Preparation of the mutant proteins of *Bst*L5

Site-directed mutagenesis was carried out by the unique site elimination method (Deng & Nickoloff, 1992), using the Chameleon™ double-stranded site-directed mutagenesis kit supplied by Stratagene. The mutagenic primers used were purchased from Amersham-Pharmacia Biotech. Mutations were confirmed by DNA sequencing using a thermo sequenase fluorescent-labeled primer cycle sequencing kit with 7-deaza dGTP (Amersham-Pharmacia Biotech) and the DSQ-1000 DNA sequencer (Shimadzu) to ensure that no alterations other than those expected had occurred. Overproduction and purification of the mutant proteins were carried out in the same manner as that described for wild-type *Bst*L5. The structural integrity was confirmed by SDS-PAGE, and CD spectra in the far-UV range 200–250 nm, as described previously (Harada et al., 1998).

ACKNOWLEDGMENTS

We thank Drs. M. Kawamoto of JASRI, and N. Kamiya, S. Adachi, and S.-Y. Park of RIKEN for their kind help with data collection using synchrotron radiation of BL41XU and BL44B2, SPring-8. This work was supported in part by a Grant-in-Aid for Scientific Research from The Ministry of Education, Science, Sports and Culture of Japan and "Ground Research for Space Utilization" promoted by NASDA and Japan Space Forum. M.Y. is supported by the Takeda Science Foundation of Japan.

Received November 21, 2000; returned for revision December 28, 2000; revised manuscript received January 26, 2001

REFERENCES

Abola EE, Sussman JL, Prilusky J, Manning NO. 1997. Protein data bank archives of three-dimensional macromolecular structures. *Methods Enzymol 276*:556–571.

Abrahams JP, Leslie AGW. 1996. Methods used in the structure determination of boivine mitochondrial F_1 ATPase. *Acta Crystallogr D52*:30–42.

Ban N, Nissen P, Hansen J, Moore PB, Steitz TA. 2000. The complete atomic structure of the large ribosomal subunit at 2.4 Å resolution. *Science 289*:905–920.

Bogdanov AA, Dontsova OA, Dokudovskaya SS, Lavrik IN. 1995. Structure and function of 5S rRNA in the ribosome. *Biochem Cell Biol 73*:869–876.

Brünger AT, Adams PD, Clore GM, Delano WL, Gros P, Grosse-Kunstleve RW, Jiang J-S, Kuszewski J, Nilges N, Pannu NS, Read RJ, Rice LM, Simonson T, Warren GL. 1998. Crystallography and NMR system (CNS): A new software system for macromolecular structure determination. *Acta Crystallogr D54*:905–921.

Burd CG, Dreyfuss G. 1994. Conserved structures and diversity of functions of RNA-binding proteins. *Science 265*:615–621.

Burge CB, Tuschl T, Sharp PA. 1999. Splicing of precursors to mRNAs by the spliceosomes. In: Gesteland RF, Cech TR, Atkins JE, eds. *The RNA world*, 2nd ed. Cold Spring Harbor, New York: Cold Spring Harbor Laboratory Press. pp 525–560.

Chen-Schmeisser U, Garrett RA. 1977. A new method for the isolation of a 5S RNA complex with proteins L5, L18, and L25 from *Escherichia coli* ribosomes. *FEBS Lett 74*:287–291.

Correll CC, Freeborn B, Moore PB, Steitz TA. 1997. Metals, motifs, and recognition in the crystal structure of a 5S rRNA domain. *Cell 91*:705–712.

Cowtain KD, Main P. 1996. Phase combination and cross validation in iterated density-modification calculations. *Acta Crystallogr D52*:43–48.

Dallas A, Rycyna R, Moore P. 1995. A proposal for the conformation of loop E in *Escherichia coli* 5S rRNA. *Biochem Cell Biol 73*:887–897.

Deng WP, Nickoloff JA. 1992. Site-directed mutagenesis of virtually any plasmid by eliminating a unique site. *Anal Biochem 200*:81–88.

Douthwaite S, Garrett RA, Wagner R, Feunteun J. 1979. A ribonuclease-resistant region of 5S RNA and its relation to the RNA binding sites of proteins L18 and L25. *Nucleic Acids Res 6*:2453–2470.

Evans PR. 1997. Scaling of MAD Data. In: Wilson KS, Davies G, Ashton AW, Baily S, eds. *Proceedings of CCP4 Study Weekend on Recent Advances in Phasing*. Daresbury, UK: Daresbury Laboratory. pp 97–102.

Garrett RA, Noller HF. 1979. Structures of complexes of 5S rRNA with ribosomal proteins L5, L18 and L25 from *Escherichia coli*: Identification of kethoxal-reactive sites on the 5S RNA. *J Mol Biol 132*:637–648.

Green R, Noller HF. 1999. Reconstitution of functional 50S ribosomes from in vitro transcripts of *Bacillus stearothermophilus* 23S rRNA. *Biochemistry 38*:1772–1779.

Harada N, Maemura K, Yamasaki N, Kimura M. 1998. Identification by site-directed mutagenesis of amino acid residues in ribosomal protein L2 that are essential for binding to 23S ribosomal RNA. *Biochim Biophys Acta 1429*:176–186.

Horne JR, Erdmann VA. 1972. Isolation and characterization of 5S RNA–protein complexes from *Bacillus stearothermophilus* and *Escherichia coli* ribosomes. *Mol Gen Genet 119*:337–344.

Huber PW, Wool IG. 1984. Nuclease protection analysis of ribonucleoprotein complexes: Use of the cytotoxic ribonuclease a-sarcin to determine the binding sites for *Escherichia coli* ribosomal proteins L5, L18, and L25 on 5S rRNA. *Proc Natl Acad Sci USA 81*:322–326.

Jones TA, Zou JY, Cowan SW, Kjeldgaard M. 1991. Improved methods for building protein models in electron density maps and the location of errors in these models. *Acta Crystallogr D49*:18–23.

Kabsch W. 1976. A solution for the best rotation to relate two sets of Vectors. *Acta Crystallogr A32*:922–923.

Kabsch W, Sander C. 1983. Dictionary of protein secondary structures: Pattern recognition of hydrogen-bonded and geometrical features. *Biopolymers 22*:2577–2637.

Khaitovich P, Mankin AS. 1999. Effect of antibiotics on large ribosomal subunit assembly reveals possible function of 5 S rRNA. *J Mol Biol 291*:1025–1034.

Kimura J, Kimura M. 1987. The complete amino acid sequences of the 5S rRNA binding proteins L5 and L18 from the moderate thermophile *Bacillus stearothermophilus* ribosome. *FEBS Lett 210*:85–90.

Kleywegt GJ, Read RJ. 1997. Not your average density. *Structure 5*:1557–1569.

La Fortelle E de, Bricogne G. 1997. Maximum-likelihood heavy-atom parameter refinement for multiple isomorphous replacement and multiwavelength anomalous diffraction methods. *Methods Enzymol 276*:472–494.

Leslie AGW. 1993. Auto-indexing of rotation diffraction images and parameter refinement. In: Sawyer L, Isaacs N, Bailey S, eds. *Proceeding of the CCP4 study weekend*. Daresbury, UK: Daresbury Laboratory. pp 44–51.

Lu M, Steitz TA. 2000. Structure of *Escherichia coli* ribosomal protein L25 complexed with a 5S rRNA fragment at 1.8-Å resolution. *Proc Natl Acad Sci USA 97*:2023–2028.

Matthews BW. 1968. Solvent content of protein crystals. *J Mol Biol 33*:491–497.

Nagai K, Oubridge C, Jessen TH, Li J, Evans PR. 1990. Crystal structure of the RNA-binding domain of the U1 small nuclear ribonucleoprotein A. *Nature 348*:515–520.

Navaza J. 1994. AmoRe: An automated package for molecular replacement. *Acta Crystallogr A50*:157–163.

Nicholls A, Sharp K, Honig B. 1991. Protein folding and association; insights from the interfacial and thermodynamic properties of hydrocarbons. *Proteins Struct Funct Genet 11*:281–296.

Nissen P, Hansen J, Ban N, Moore PB, Steitz TA. 2000. The structural basis of ribosome activity in peptide bond synthesis. *Science 289*:920–930.

Oubridge C, Ito N, Evans PR, Teo C-H, Nagai K. 1994. Crystal structure at 1.92 Å resolution of the RNA-binding domain of the U1A spliceosomal protein complexed with an RNA hairpin protein complexed with an RNA hairpin. *Nature 372*:432–438.

Ramakrishnan V, White SW. 1998. Ribosomal protein structures: Insights into the architecture, machinery and evolution of the ribosome. *Trends Biochem Sci 23*:208–212.

Read RJ. 1986. Improved Fourier coefficients for maps using phases from partial structures with errors. *Acta Crystallogr A42*:140–149.

Schulze H, Nierhaus KH. 1982. Minimal set of ribosomal components for reconstitution of the peptidyltransferase activity. *EMBO J 1*:609–613.

Schwarzbauer J, Craven GR. 1981. Apparent association constants for *E. coli* ribosomal proteins S4, S7, S8, S15, S17, and S20 binding to 16S RNA. *Nucleic Acids Res 9*:2223–2237.

Sergiev PV, Bogdanov AA, Dahlberg AE, Dontsova O. 2000. Mutations at position A960 of *E. coli* 23 S ribosomal RNA influence the structure of 5 S ribosomal RNA and the peptidyltransferase region of 23 S ribosomal RNA. *J Mol Biol 299*:379–389.

Shpanchenko OV, Zvereva MI, Dontsova OA, Nierhaus KN, Bogdanov AA. 1996. 5S rRNA sugar-phosphate backbone protection in complexes with specific ribosomal proteins. *FEBS Lett 394*:71–75.

Shpanchenko OV, Dontsova OV, Bogdanov AA, Niehaus KH. 1998. Structure of 5S rRNA within the *Escherichia coli* ribosome: Iodine-induced cleavage patterns of phosphorothioate derivatives. *RNA 4*:1154–1164.

Stoldt M, Wohnert J, Gorlach M, Brown LR. 1998. The NMR structure of *Escherichia coli* ribosomal protein L25 shows homology to general stress proteins and glutaminyl-tRNA synthetases. *EMBO J 17*:6377–6384.

Stoldt M, Wohnert J, Ohlenschlager O, Gorlach M, Brown LR. 1999. The NMR structure of the 5S rRNA E-domain-protein L25 complex shows preformed and induced recognition. *EMBO J 18*:6508–6521.

Terwilliger TC, Berendzen J. 1999. Automated MAD and MIR structure solution. *Acta Crystallogr D55*:849–861.

Zimmermann J, Erdmann VA. 1978. Identification of *Escherichia coli* and *Bacillus stearothermophilus* ribosomal protein binding sites on *Escherichia coli* 5S rRNA. *Mol Gen Genet 160*:247–257.